CHEMISTRY
A EUROPEAN JOURNAL

DOI: 10.1002/chem.201000128

Cyanide-Bridged $[Co^{II}_2M^{II}]$ and $[Co^{II}_2M^{II}_2]$ Complexes Based on the $[Co^{II}(triphos)(CN)_2]$ Building Block: Syntheses, Structures, Magnetic Properties, and Density Functional Theoretical Studies

Ferdi Karadas,[a] Michael Shatruk,[b] Lisa M. Perez,[a] and Kim R. Dunbar*[a]

Abstract: Two families of cationic cyanide-bridged complexes, namely, $\{[Co(triphos)(CN)_2]_2[M(MeOH)_4]\}(ClO_4)_2$ ($[Co_2M]$ M = Mn, Fe, Co, and Ni; triphos = 1,1,1-tris((diphenylphosphino)-methyl)ethane) and $\{[Co(triphos)(CN)_2]_2[M(MeOH)_4]_2\}(ClO_4)_4$ ($[Co_2M_2]$ M = Mn and Ni) have been prepared from reactions of $[Co^{II}(triphos)(CN)_2]$ and $M(ClO_4)_2{\cdot}6H_2O$ (M = Mn, Fe, Co, Ni) in methanol. The trinuclear complexes $[Co_2Mn]$, $[Co_2Fe]$, and $[Co_2Co]$, as well as both new tetranuclear complexes $[Co_2Mn_2]$ and $[Co_2Ni_2]$, exhibit antiferromagnetic coupling between metal centers. In contrast, the $[Co_2Ni]$ is characterized by ferromagnetic interactions between the Co^{II} and Ni^{II} centers. The magnetic behavior for these complexes was investigated by DFT calculations and was found to derive from overlap patterns of the different magnetic orbitals as influenced by the angles of the cyanide bridges.

Keywords: cobalt · cyanides · density functional calculations · magnetic properties · X-ray diffraction

Introduction

Cyanide chemistry is a convenient route to compounds with diverse properties.[1,2] In particular, research efforts over the past decade have led to the isolation of many discrete cyanide molecules with fascinating magnetic properties.[2] Extensive spectroscopic, electrochemical, and occasionally theoretical studies, have provided valuable insight into the nature of the photophysical, electronic, and magnetic properties of cyanide compounds.

Among the advantages to using the cyanide ligand to build magnetic architectures are that both the structures and superexchange interactions between metal centers that are bound in an end-to-end fashion can typically be predicted. Specifically, it is known that in most cases unpaired electrons in orbitals of octahedrally coordinated metal centers in the M–CN–M' pair couple antiferromagnetically if the orbital mixing is symmetry-allowed (t_{2g}–t_{2g} or e_g–e_g) and ferromagnetically if the orbitals are orthogonal to each other (t_{2g}–e_g). Although these principles of magnetic coupling for octahedral metal ions have been amply verified by experimental observations, relatively little is known about coupling through cyanide for other metal ion geometries.[2] Changes in the coordination environment can alter the disposition of the magnetic orbitals and, consequently, the nature of magnetic superexchange,[17–19] as nicely illustrated by a series of dinuclear cyanide-bridged Cu^{II} complexes in which the Cu^{II} centers adopt a trigonal-bipyramidal coordination geometry. The superexchange values (J) for a series of these clusters vary over an order of magnitude, a result that has been explained on the basis of a difference in the orientation of the d_{z^2} magnetic orbital, a conclusion that was supported by theoretical studies.[3]

A common strategy in cyanide magnetochemistry research is to design suitable precursors equipped with one or more cyanide ligands as well as capping groups and to react such building blocks with metal complexes that possess open sites or substitutionally labile ligands. The nature of the resulting compound is governed by the geometry of the reactants, with the less soluble neutral product(s) typically being favored. The majority of known cyanide magnetic clusters prepared in this manner have all of their cyanide ligands involved in bridging interactions, with the remaining coordination sites being occupied by a polydentate ligand:

[a] Dr. F. Karadas, Dr. L. M. Perez, Prof. K. R. Dunbar
Department of Chemistry, Texas A&M University
P.O. Box 30012, College Station, TX 77842-3012 (USA)
Fax: (+1) 979-845-7177
E-mail: dunbar@mail.chem.tamu.edu

[b] Prof. M. Shatruk
Department of Chemistry & Biochemistry
Florida State University, Tallahassee, FL 32306 (USA)

Supporting information for this article is available on the WWW under http://dx.doi.org/10.1002/chem.201000128.

WILEY InterScience DISCOVER SOMETHING GREAT
© 2010 Wiley-VCH Verlag GmbH & Co. KGaA, Weinheim

examples of such complexes are $\{[Cu^{II}(tpa)]_4[Ni^{II}(CN)_4]\}(ClO_4)_6$[20] and $\{[(bpy)_2Fe^{II}(CN)_2]_2[Fe^{II}(tpa)]_2\}(BF_4)_4$[21] by Vahrenkamp et al. (tpa = tris(2-pyridylmethyl)amine, bpy = 2,2′-bipyridine), $\{[(bpy)_2Fe^{II}(CN)_2]_2[Co^{II}(bpy)_2]_2\}(PF_6)_4$ by Oshio et al.,[22] $\{[(triphos)Re^{II}(CN)_3]_4[Mn^{II}Cl]_4\}$ by Dunbar et al. (triphos = 1,1,1-tris((diphenylphosphino)methyl)-ethane),[23] and $\{[(tacn)Co^{III}(CN)_3]_4[Cr^{III}(tacn)]_4\}OTf_{12}$[24] and $\{[(Me_3tacn)Cu^{II}]_3[TpFe^{III}(CN)_3]_2\}(ClO_4)_4$[25] (tacn = 1,4,7,-triazacyclononane, Tp = hydrotris(1-pyrazolyl)borate) by Long et al. A less common class comprises neutral clusters with dangling cyanide and/or labile ligands that are accessible for further reactions such as $\{[(bpy)Cr^{III}(CN)_4]_2[Mn^{II}(H_2O)_4]\}$ by Julve et al.,[26] $\{[(Tp)Fe^{III}(CN)_3]_2[Mn^{II}(MeOH)_4]\}$ by Gao et al.,[27] and $\{[(bpy)W^{V}(CN)_6]_2[Co^{II}(dmso)_4]\}$ by Hong et al.[28]

Another more challenging, but attractive, strategy to access discrete mixed-metal cyanide molecules is to prepare clusters that are charged rather than neutral, and which contain reactive sites that allow entry into systematic preparation of higher nuclearity clusters. One of our strategies to this end has been to use the pentacoordinate neutral molecule $[Co^{II}(triphos)(CN)_2]$[29,30] as, for example, in reactions with 3d metal-ion chlorides to prepare molecular squares of general formula $\{[Co^{II}(triphos)(CN)_2]_2[MCl_2]_2\}$ (M = Mn, Fe, Co, Ni, Zn).[31,32] Magnetic studies revealed that antiferromagnetic coupling occurs between the square-pyramidal low-spin Co^{II} centers ($S = 1/2$) and the tetrahedral metal ions in this family of cyanide-bridged clusters.

A logical extension of the aforementioned chemistry is to introduce capping solvent molecules in place of the chlorides. This chemistry resulted in the isolation of two new types of trinuclear and tetranuclear cyanide-bridged clusters, the syntheses, structures, and magnetic properties of which are reported herein. To augment our understanding of the experimental data, DFT calculations were performed to gain insight into the nature of the different magnetic interactions observed for the analogs containing the Co^{II}–CN–Ni^{II} unit.

Experimental Section

Physical measurements: IR spectra were measured as Nujol mulls placed between KBr plates on a Nicolet 740 FT-IR spectrometer. Magnetic measurements were performed on crushed polycrystalline samples with a Quantum Design SQUID magnetometer MPMS-XL. DC magnetic susceptibility measurements were carried out in an applied field of 1000 G in the 2–300 K range. Magnetization data were collected at 1.8 K with the magnetic field varying from 0 to 7 Tesla. Field- and temperature-dependent magnetization data were collected in the 1.8–3.9 K temperature range in fields of 1–7 Tesla. The data were corrected for diamagnetic contributions calculated from the Pascal constants.

Computational studies: The molecular and electronic structure calculations were performed by DFT methods by using the Gaussian 03 (G03) program package.[33] The B3LYP[34–36] functional along with the 6–31G* basis set was used for H, C, N, and O,[37] along with the Couty–Hall Modified LANL2DZ basis sets[38] for transition-metal ions. Hydrogen atoms were used in place of phenyl groups of the triphos ligand in the computational models. All geometries were fully optimized under the conditions of the respective programs. Orbital analysis was completed with Molekel 4.3.[39]

Syntheses

Starting materials: The starting materials $Mn(ClO_4)_2{\cdot}6H_2O$, $Fe(ClO_4)_2{\cdot}6H_2O$, $Co(BF_4)_2{\cdot}6H_2O$, $Ni(ClO_4)_2{\cdot}6H_2O$, triphos, and anhydrous $CoCl_2$ were purchased from Aldrich and used as received. The precursors $[Co(triphos)(CN)_2]$,[29] $[Mn(CH_3CN)_4](BF_4)_2$,[40] and $[Ni(CH_3CN)_6](BF_4)_2$[40] were prepared according to the reported procedures. All solvents were dried by standard methods and handled anaerobically.

$\{[Co(triphos)(CN)_2]_2[Mn(MeOH)_4]\}(BF_4)_2$ $[Co_2Mn]$: A colorless solution of $[Mn(CH_3CN)_4](BF_4)_2$ (54 mg, 0.138 mmol) in methanol (15 mL) was slowly added to a claret solution of $[Co(triphos)(CN)_2]$ (202 mg, 0.277 mmol) in methanol (20 mL) under N_2. The mixture was left to stand undisturbed for 3–4 d. Dark-red crystals of $[Co_2Mn]{\cdot}2H_2O$ that had formed were collected by filtration and washed with methanol/diethyl ether (10 mL, 1:1 v/v) followed by a copious amount of diethyl ether (yield = 40 %). IR (Nujol): $\tilde{\nu}(C{\equiv}N) = 2121$ (s), 2094 cm^{-1} (s); elemental analysis calcd (%) for $[Co_2Mn]$ $Co_2MnC_{90}H_{94}N_4P_6O_4B_2F_8$: C 59.10, H 5.18, N 3.07, O 3.50; found: C 58.98, H 5.32, N 3.12, O 3.65.

$\{[Co(triphos)(CN)_2]_2[M(MeOH)_4]\}(BF_4)_2$ (M = Fe, Co, Ni), $[Co_2Fe]$, $[Co_2Co]$, and $[Co_2Ni]$: These complexes were prepared by using an analogous procedure to that for $[Co_2Mn]$ with the specific corresponding metal salts. The isolated yields were 28, 32, and 46 %, respectively. The single crystals of $[Co_2Fe]{\cdot}3H_2O$, $[Co_2Co]{\cdot}CH_3OH$, and $[Co_2Ni]{\cdot}2CH_3OH$ were obtained in the same manner as described for $[Co_2Mn]{\cdot}2H_2O$. IR (Nujol) for $[Co_2Fe]$: $\tilde{\nu}(C{\equiv}N) = 2131$ (s), 2094 cm^{-1} (s); IR (Nujol) for $[Co_2Co]$: $\tilde{\nu}(C{\equiv}N) = 2134$ (s), 2094 cm^{-1}(s); IR (Nujol) for $[Co_2Ni]$: $\tilde{\nu}(C{\equiv}N) = 2138$ (s), 2094 cm^{-1} (s); elemental analysis calcd (%) for $[Co_2Fe]$ $Co_3C_{90}H_{94}N_4P_6O_4B_2F_8$: C 59.07, H 5.18, N 3.06, O 3.50; found: C 58.49, H 5.24, N 3.02, O 3.82; elemental analysis calcd (%) for $[Co_2Co]$ $Co_3C_{90}H_{94}N_4P_6O_4B_2F_8$: C 58.21, H 5.11, N 3.02, O 10.34, Cl 3.77; found: C 57.88, H 5.23, N 2.94, O 10.98, Cl 3.69; elemental analysis calcd (%) for $[Co_2Ni]$ $Co_3C_{90}H_{94}N_4P_6O_4B_2F_8$: C 58.24, H 5.11, N 3.02, O 10.35, Cl 3.77; found: C 57.73, H 5.28, N 2.92, O 10.68, Cl 3.62.

$\{[Co(triphos)(CN)_2]_2[Mn(MeOH)_4]_2\}(BF_4)_4$ $[Co_2Mn_2]$: A claret solution of $[Co(triphos)(CN)_2]$ (202 mg, 0.277 mmol) in methanol (20 mL) was added dropwise to a colorless solution of $[Mn(CH_3CN)_4](BF_4)_2$ (108 mg, 0.277 mmol) in methanol (15 mL) under N_2 at −42 °C. The mixture was left to stand undisturbed for 1 d. Dark-red crystals of $[Co_2Mn_2]{\cdot}4CH_3OH$ that formed were filtered, washed with methanol/diethyl ether (12 mL, 1:2 v/v), and finally washed with a copious amount of diethyl ether (yield = 22 %). IR (Nujol): $\tilde{\nu}(C{\equiv}N) = 2132$ (s), 2106 cm^{-1} (w); elemental analysis calcd (%) for $[Co_2Mn_2]$ $Co_2Mn_2C_{94}H_{110}N_4P_6O_8B_4F_{16}$: C 51.64, H 5.08, N 2.56, O 5.86; found: C 51.44, H 5.16, N 2.48, O 6.09.

$\{[Co(triphos)(CN)_2]_2[Ni(MeOH)_4]_2\}(BF_4)_4$ $[Co_2Ni_2]$: $[Co_2Ni_2]$ was prepared as described above for $[Co_2Mn_2]$ (yield = 28 %). IR (Nujol): $\tilde{\nu}(C{\equiv}N) = 2148$ (s), 2106 cm^{-1} (w); elemental analysis calcd (%) for $[Co_2Ni_2]$ $Co_2Ni_2C_{94}H_{110}N_4P_6O_8B_4F_{16}$: C 51.50, H 5.06, N 2.56, O 5.84; found: C 51.22, H 5.09, N 2.59, O 6.16.

X-ray crystallography: In a typical experiment, a crystal selected for study was suspended in polybutene oil (Aldrich) and mounted on a cryoloop, which was placed in an N_2 cold stream. Single-crystal X-ray data for all complexes were collected on a Bruker APEX diffractometer at 110 K. The data sets were recorded as three ω-scans of 606 frames each at 0.3° stepwidth, and integrated with the Bruker SAINT software package.[41] For each complex, the data set was indexed in a monoclinic unit cell and systematic extinctions indicated the space group to be $P2_1/n$ for $[Co_2M]$ and $C2/c$ for $[Co_2M_2]$. An absorption correction (SADABS)[42] was based on fitting a function to the empirical transmission surface as sampled by multiple equivalent measurements. Solution and refinement of the crystal structures was carried out by using the SHELX suite of programs and X-SEED,[43] a graphical interface. Structure solution by direct methods resolved positions of all metal atoms and most of the lighter atoms. The remaining non-hydrogen atoms were located by alternating cycles of least-squares refinements and difference Fourier maps. The final refinements were carried out with anisotropic thermal parameters for all non-hydrogen atoms. A summary of pertinent information relating to unit cell, data collection, and refinement parameters is provided

 © 2010 Wiley-VCH Verlag GmbH & Co. KGaA, Weinheim

Table 1. Crystal data and details of the structure determination for the trinuclear salts, $[Co_2M]$.

	$[Co_2Mn]\cdot 2H_2O$	$[Co_2Fe]\cdot 3H_2O$	$[Co_2Co]\cdot CH_3OH$	$[CoNi]\cdot CH_3OH$
formula	$Co_2MnC_{90}H_{90}P_6N_4O_{10}B_2F_8$	$Co_2FeC_{90}H_{98}P_6N_4O_8B_2F_8$	$Co_3C_{92}H_{100}P_6N_4O_{14}Cl_2$	$Co_2NiC_{92}H_{102}P_6N_4Cl_2O_{14}$
space group	$P2_1/n$ (No. 14)	$P2_1/n$ (No. 14)	$P2_1/n$ (No. 14)	$P2_1/n$ (No. 14)
a [Å]	11.207(5)	11.17(2)	11.209(1)	11.402(3)
b [Å]	18.54(2)	18.53(2)	18.553(2)	19.250(5)
c [Å]	21.68(1)	21.70(3)	21.694(2)	20.784(5)
β [°]	96.37(2)	96.90(2)	96.454(4)	99.76(1)
V [Å^3]	4475(4)	4461(10)	4482.9(7)	4496(2)
Z	2	2	2	2
ρ_{calcd} [g cm^{-3}]	1.425	1.412	1.422	1.419
μ [mm^{-1}]	0.689	0.710	0.733	0.803
crystal color and habit	dark-red block	dark-red plate	blue plate	green-blue plate
crystal size [mm]	$0.21\times0.18\times0.17$	$0.22\times0.16\times0.13$	$0.12\times0.11\times0.08$	$0.19\times0.17\times0.12$
T [K]	110(2)	110(2)	108(2)	110(2)
λ ($Mo_{K\alpha}$) [Å]	0.71073	0.71073	0.71073	0.71073
min and max θ [°]	1.45 to 28.27	1.45 to 28.65	3.14 to 39.25	1.91 to 28.30
total reflns	37198	36086	8267	39800
independent reflns	10733	10521	2329	10936
data/parameters/restraints	10733/320/0	10521/320/0	2329/421/0	10936/320/0
R_1 [$F_o > 4\sigma(F_o)$]	0.0551	0.0832	0.0629	0.0553
wR_2	0.1503	0.2036	0.2260	0.1305
max/min residual densities [e Å^{-3}]	1.133/−0.966	1.083/−1.191	0.442/−0.588	2.242/−0.769

Table 2. Selected bond lengths [Å] and angles [°] for the trinuclear salts $[Co_2M]$.

Parameters	$[Co_2Mn]$	$[Co_2Fe]$	$[Co_2Co]$	$[Co_2Ni]$
Co1−C1	1.886(3)	1.877(6)	1.90(2)	1.877(3)
Co1−C2	1.908(3)	1.906(6)	1.91(2)	1.900(3)
Co1−P1	2.2422(13)	2.227(3)	2.236(5)	2.2473(9)
Co1−P2	2.2154(13)	2.219(2)	2.215(5)	2.2277(10)
Co1−P3	2.2800(13)	2.285(3)	2.277(6)	2.2799(9)
M1−N1	2.107(3)	2.074(5)	2.023(14)	2.020(3)
M1−O1	2.129(3)	2.119(4)	2.094(14)	2.089(2)
M1−O2	2.144(3)	2.119(5)	2.089(10)	2.090(3)
C1-Co1-C2	83.61(14)	83.2(2)	84.1(7)	80.78(13)
C1-Co1-P2	161.99(10)	161.96(7)	161.2(5)	160.95(9)
C2-Co1-P2	88.19(10)	88.47(18)	88.0(6)	90.39(9)
C1-Co1-P1	94.03(10)	94.35(17)	93.8(5)	92.92(9)
C2-Co1-P1	164.49(10)	164.12(18)	164.9(6)	167.94(12)
P2-Co1-P1	89.59(4)	89.26(6)	89.4(2)	89.09(3)
C1-Co1-P3	101.95(10)	101.97(19)	102.8(5)	101.59(10)
C2-Co1-P3	107.47(10)	107.46(19)	107.1(6)	109.14(9)
P2-Co1-P3	95.79(3)	95.78(10)	95.8(2)	92.44(3)
P1-Co1-P3	88.02(4)	88.41(8)	88.00(19)	90.33(4)
C1-N1-M1	146.7(3)	148.4(4)	152.2(13)	156.9(3)
Co1-C1-N1	169.6(3)	169.6(5)	165.9(5)	170.2(3)

in Tables 1 and 3. Selected metal–ligand bond lengths are listed in Tables 2 and 4.

Results and Discussion

Syntheses: Reactions of the mononuclear precursor [Co(triphos)$(CN)_2$] with hydrated salts of 3d transition-metal ions result in the formation of both trinuclear and tetranuclear cyanide-bridged molecules. The nuclearity of the resulting compound depends on the stoichiometric ratio of the reactants, the counterion, and the temperature of the reaction medium. The reaction of [Co(triphos)$(CN)_2$] and M$(ClO_4)_2\cdot 6H_2O$ in a 2:1 ratio yields trinuclear clusters of general formula $\{[Co(triphos)(CN)_2]_2[M(MeOH)_4]\}X_2$ (M = Mn, Fe, Co, Ni; X = ClO_4^-, BF_4^-). If the reaction is performed in a 1:1 ratio the result is the same, namely, a mixture of the trinuclear complex and a tetranuclear cluster $\{[Co(triphos)(CN)_2]_2[M(MeOH)_4]_2\}(BF_4)_4$ is obtained. Efforts to isolate the tetranuclear cluster by using an excess of the transition-metal ion M^{II} also led to the mixture of aforementioned clusters, which can be explained by the higher solubility of the tetranuclear complexes in polar solvents. Consequently, the reactions were performed at low temperatures to decrease the solubility of the tetranuclear clusters. Slow diffusion of methanol solutions of [Co(triphos)$(CN)_2$] and M$(BF_4)_2$ in a 1:1 ratio at −42 °C resulted in the formation of crystals of only the tetranuclear products. Both the trinuclear and tetranuclear complexes are soluble in common polar solvents such as CH_2Cl_2, CH_3OH, and CH_3CN.

In terms of related trinuclear cyanide-bridged clusters, there are previously reported examples in which the central metal ion is surrounded by four solvent molecules in addition to two nitrogen atoms from cyanide bridges. The most widely investigated class are those with the $[Fe^{III}{}_2Mn^{II}]$ metal core prepared by reacting $[Fe^{III}(CN)_3(L_3)]$ (L_3 = Tp^-,[27] 8-(pyridine-2-carboxamido)quinoline (pcq^-),[44] or bis(2-pyridylcarbonyl)amidate ($bpca^-$))[45] with solvated Mn^{II} ions.

Single-crystal X-ray structural studies: The structures of the $[Co_2M]$ clusters (Figure 1a) consists of a central octahedral M^{II} ion that resides on a crystallographic inversion center and which is bonded to four methanol molecules in the equatorial plane. Two [Co(triphos)$(CN)_2$] units are connected to the M^{II} center in a *trans* fashion. The Co^{II} sites retain their pentacoordinate square-pyramidal geometry in which one of the phosphorus atoms occupies the axial position and two carbon atoms of the cyanide and the two remaining

 © 2010 Wiley-VCH Verlag GmbH & Co. KGaA, Weinheim

Table 3. Crystal data and details of the structure determination for the tetranuclear salts $[Co_2M_2]$.

	$[Co_2Mn_2]\cdot 4CH_3OH$	$[Co_2Ni_2]\cdot 2CH_3OH$
formula	$Co_2Mn_2C_{98}H_{100}P_6N_4O_{12}B_4F_{16}$	$Co_2Ni_2C_{96}H_{104}P_6N_4O_{10}B_4F_{16}$
space group	*C*2/*c*	*C*2/*c*
a [Å]	27.2420(6)	27.210(5)
b [Å]	14.560(3)	14.180(3)
c [Å]	30.730(6)	31.030(6)
β [°]	105.08(3)	105.82(3)
V [Å^3]	11846(4)	11808(4)
Z	4	4
ρ_{calcd} [g cm^{-3}]	1.282	1.257
μ [mm^{-1}]	0.643	0.744
crystal color and habit	dark-red block	dark-red block
crystal size [mm]	$0.21\times0.18\times0.17$	$0.22\times0.18\times0.14$
T [K]	110(2)	110(2)
λ ($Mo_{K\alpha}$) [Å]	0.71073	0.71073
min and max θ [°]	1.37 to 28.38	1.48 to 27.88
total reflns	59124	59058
independent reflns	14467	13492
data/parameters/restraints	14467/713/10	13492/670/10
R_1 [$F_o > 4\sigma(F_o)$]	0.0789	0.0886
wR_2	0.2623	0.3016
max/min residual densities [e Å^{-3}]	2.015/−0.913	2.399/−1.818

Table 4. Selected bond lengths [Å] and angles [°] for the tetranuclear salts $[Co_2M_2]$.

Parameters	$[Co_2Mn_2]$	$[Co_2Ni_2]$
Co1−C1	1.894(4)	1.914(5)
Co1−C2	1.896(5)	1.907(8)
Co1−P1	2.2375(12)	2.2365(11)
Co1−P2	2.2952(13)	2.2919(14)
Co1−P3	2.2229(13)	2.2262(16)
M1−O1	2.134(4)	2.098(6)
M1−O2	2.129(3)	2.102(5)
M1−O3	2.189(5)	2.086(5)
M1−O4	2.217(4)	2.194(5)
M1−N1	2.158(4)	2.104(4)
M1−N2	2.156(4)	2.115(5)
C1-Co1-C2	85.28(19)	85.0(2)
C1-Co1-P3	91.48(14)	91.68(16)
C2-Co1-P3	164.51(15)	164.52(17)
C1-Co1-P1	164.98(14)	164.88(16)
C2-Co1-P1	90.33(13)	90.40(15)
C1-Co1-P2	102.55(14)	102.64(16)
C2-Co1-P2	106.55(15)	106.54(17)
C1-N1-M1	168.2(4)	167.9(4)
Co1-C1-N1	175.1(4)	175.4(5)

phosphorus atoms occupy the equatorial positions of the square pyramid, in a manner akin to the $[Co(triphos)(CN)_2]$ molecule. The C-Co-C angles range from 80.8 to 84.1°, which are more acute than those of the mononuclear precursor (87.6°) and the corresponding angles in the series of molecular squares, $\{[Co^{II}(triphos)(CN)_2]_2[MCl_2]_2\}$ ($\approx$85°). The reduction in the C-Co-C angle is due to a hydrogen-bonding interaction (the H···N distance is $\approx$1.98 Å) between the hydrogen atom of one of the methanol molecules connected to the central M^{II} ion and the nitrogen lone pair of the dangling cyanide ligand (Figure 2). This hydrogen-bonding interaction also causes the C-N-M angle to deviate significantly from 180° (they vary from 146.7 to 156.9°). It was found that the magnitude of the angle affects the magnetic exchange across the cyanide bridge, a fact that will be discussed in the computational section (see Table 5).

The tetranuclear complexes $[Co_2M_2]$ are composed of alternating $[Co(triphos)(CN)_2]$ and $[M(MeOH)_4]^{2+}$ fragments to give a cationic cluster with a 4+ charge (Figure 1b). The molecules crystallize on inversion centers. The bridging cyanide ligands are connected to the M^{II} centers in a *cis* fashion, in contrast to the *trans* arrangement in the trinuclear clusters described above. The C-Co-C angle is approximately 85°, whereas the N-M-N angle is approximately 97°. Because all the cyanide ligands are bridging in these molecules, there are no hydrogen-bonding interactions. As a result, the C-N-M angle (167°) does not deviate as much from 180° as compared with the angle in the $[Co_2M]$ clusters (146.7–156.9°). Consequently, the $Co^{II}\cdots M^{II}$ distance ($\approx$5.12 Å) is longer than the corresponding values in the $[Co_2M]$ clusters ($\approx$4.81 Å).

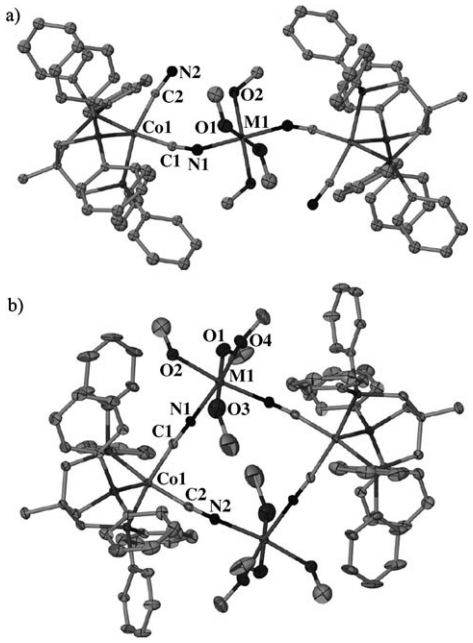

Figure 1. a) Molecular structure of the trinuclear complexes $[Co_2M]$ plotted from X-ray coordinates (complex $[Co_2Ni]$ was used to make the figure). b) Molecular structure of the tetranuclear complexes $[Co_2M_2]$ in which M = Mn, Ni (complex $[Co_2Ni_2]$ was used to make the figure). Hydrogen atoms are omitted for clarity. Thermal ellipsoids are projected at the 50% probability level.

 © 2010 Wiley-VCH Verlag GmbH & Co. KGaA, Weinheim

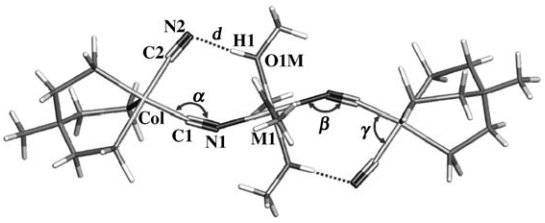

Figure 2. Stick diagram of the trinuclear complexes indicating the presence of hydrogen bonding between the atoms N2 and H1.

Table 5. Bond lengths [Å] and angles [°] displayed in Figure 2.

Complex	N2···H1 (d)	Co1-C1-N1 (α)	M1-N1-C1 (β)	C1-Co1-C2 (γ)
[Co_2Mn]	1.992	169.6	146.7	83.6
[Co_2Fe]	1.982	169.6	148.4	83.2
[Co_2Co]	2.091	165.9	152.2	84.0
[Co_2Ni]	2.052	170.2	156.8	80.8

Infrared spectral studies: Polycrystalline samples of the complexes exhibit distinctive stretching modes for the cyanide ligand in the frequency range of 2000–2200 cm^{-1}. The trinuclear complexes exhibit two $\tilde{\nu}$(C≡N) stretches located at 2121 (s) and 2094 cm^{-1} (s) for [Co_2Mn], 2131 (s) and 2094 cm^{-1} (s) for [Co_2Fe], 2134 (s) and 2094 cm^{-1} (s) for [Co_2Co], and 2138 (s) and 2094 cm^{-1} (s) for [Co_2Ni]. The stretch located at 2094 cm^{-1}, which is common for all of these complexes, is assigned to the dangling cyanide ligands, whereas the features at higher frequency are attributed to bridging cyanides.

The tetranuclear complexes exhibit two stretches located at 2132 (s) and 2106 cm^{-1} (w) for [Co_2Mn] and 2148 (s) and 2106 cm^{-1} (w) for [Co_2Ni], which are similar to the previously reported data for the tetranuclear complexes of the type {[Co^{II}(triphos)$(CN)_2$][MCl_2]}.[32] The $\tilde{\nu}$(C≡N) stretches of the [Co_2M_2] complexes appear at higher frequencies as compared with those observed for the trinuclear family. We attribute this fact to stronger back-bonding between the cyanide ligand and the octahedral metal center because the C-N-M angle in the tetranuclear clusters (167°) is much closer to 180° than the angles for the trinuclear family of complexes (≈150°).

Magnetic properties: Magnetic susceptibility measurements were performed on crushed polycrystalline samples in the temperature range of 2–300 K at an applied magnetic field of 1000 Oe. The DC magnetic susceptibility measurements of the precursor, [Co(triphos)$(CN)_2$], have been discussed previously.[32] The χT value is 0.41 emu mol^{-1} K at 300 K and remains constant over the entire temperature range of 2–300 K. Such behavior is typical of a simple paramagnet with an $S=1/2$ ground state and $g=2.10$. This g value was kept fixed for the low-spin Co^{II} centers for the purposes of modeling the magnetic properties of the tri- and tetranuclear complexes as discussed below.

{[Co(triphos)$(CN)_2$]$_2$[M$(MeOH)_4$]}$(ClO_4)_2$ (M = Mn, Fe, Co, Ni): The room-temperature χT value for [Co_2Mn] is 5.11 emu mol^{-1} K, which is close to that expected for two low-spin Co^{II} ions ($S=1/2$, $\chi T=0.41$) and one high spin Mn^{II} ion in the absence of magnetic coupling. The χT value continuously decreases upon cooling and reaches a minimum of 1.85 emu mol^{-1} K at 4 K, indicating the presence of antiferromagnetic interactions between the Co^{II} and Mn^{II} centers (Figure 3). An examination of the ground-state spin for

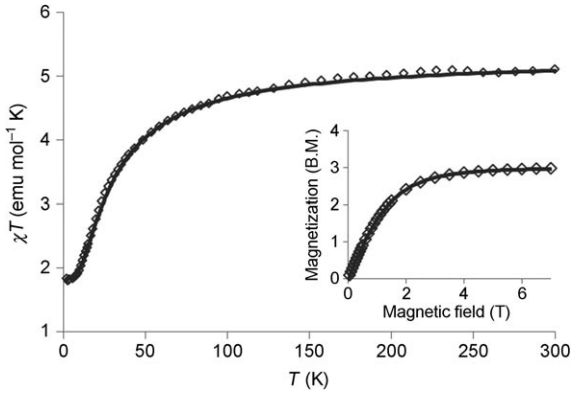

Figure 3. Temperature dependence of the χT product for [Co_2Mn]. Inset: Field dependence of magnetization at 1.8 K. The solid lines represent a simulation by using MAGPACK.

[Co_2Mn] was carried out by performing field-dependent magnetization measurements at 1.8 K. The magnetization curve approaches a saturation value of 2.98 μ_B in accordance with the ground state spin value of $S=3/2$ expected from antiferromagnetic coupling. The simulation of the magnetic data was carried out by using MAGPACK, by applying the Hamiltonian described in Equation (1) in the limit of isotropic exchange interactions in which g_{Co} was fixed at 2.10, as found for the mononuclear [Co(triphos)$(CN)_2$] precursor, H_z is the magnetic field, J is the magnetic exchange constant, and D is the zero-field splitting (zfs) parameter.

$$\mathcal{H} = \mu_B H_z(2g_{Co}S_{z,Co} + g_M S_{z,M}) - 2J(S_{Co1} + S_{Co2}) \cdot (S_M) + D_M[S^2{}_{z,M} - 1/3S_M(S_M + 1)] \quad (1)$$

The best agreement was obtained with $g_{Mn}=2.02$, $D_{Mn}=-0.13$ cm^{-1}, and $J=-4.8$ cm^{-1}. The field- and temperature-dependent magnetization data were satisfactorily simulated with ANISOFIT[46] for the $S=3/2$ ground state with $D_{GS}=-0.08$ cm^{-1} (Figure S1 in the Supporting Information).

The room-temperature χT value for [Co_2Fe] is 4.86 emu mol^{-1} K, which is higher than the expected spin-only value of 3.9 emu mol^{-1} K for two isolated low-spin Co^{II} centers and a high-spin Fe^{II} center. The deviation is rationalized by an orbital contribution from the $S=2$ Fe^{II} ion (Figure 4a). The χT value decreases slowly upon cooling down to 20 K and then decreases more abruptly below 20 K owing

 © 2010 Wiley-VCH Verlag GmbH & Co. KGaA, Weinheim

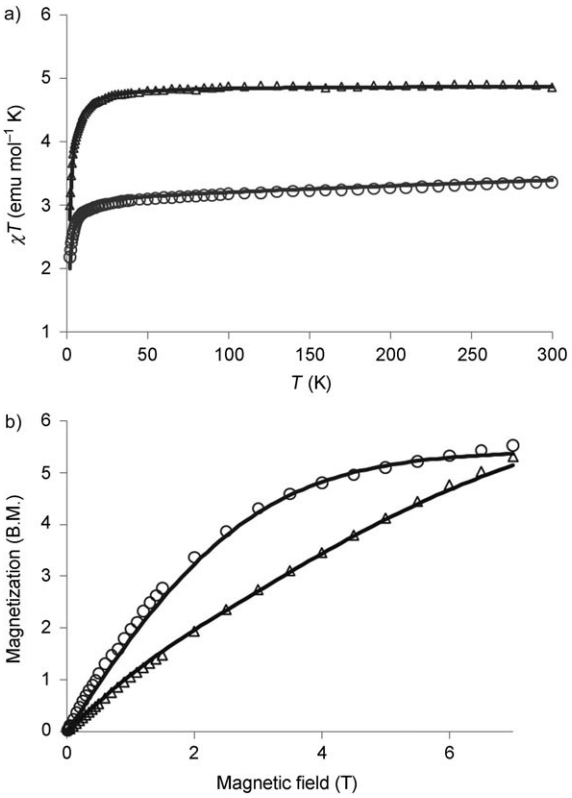

Figure 4. a) Temperature dependence of the χT product for $[Co_2Co]$ (○) and $[Co_2Fe]$ (△). b) Field dependence of magnetization for $[Co_2Co]$ (○) and $[Co_2Fe]$ (△) at 1.8 K. The solid lines represent a simulation by using MAGPACK.

to zfs effects to reach a minimum of 3.00 emu mol^{-1}K at 1.8 K. The magnetization curve recorded at 1.8 K shows a gradual increase in the magnetization value that does not exhibit saturation; the maximum is 5.31 μ_B at 7 T. Both temperature- and field-dependent behavior suggest that magnetic exchange between the Co^{II} and Fe^{II} ions is rather weak. Indeed, by using the Hamiltonian from Equation (1), the best fit to the experimental data was obtained with $g_{Fe}=2.20$, $D_{Fe}=-2.7$ cm^{-1}, and $J=-0.6$ cm^{-1}. An examination of field-dependent magnetization data at different temperatures revealed that the $[Co_2Fe]$ cluster is characterized by significant magnetic anisotropy (Figure S2 in the Supporting Information).

In the case of the $[Co_2Co]$ complex, χT exhibits values of 3.36 emu mol^{-1}K at 300 K and 2.18 emu mol^{-1}K at 1.8 K (Figure 4a). The room-temperature value is higher than the spin-only value of 2.7 emu mol^{-1}K expected for two $S=1/2$ Co^{II} and one $S=3/2$ Co^{II} centers in the absence of magnetic interaction. This deviation is caused by the typical orbital contribution of the high-spin Co^{II} ion. Similar to the $[Co_2Fe]$ cluster, the magnetization curve at 1.8 K does not exhibit saturation and reaches the maximum value of 5.53 μ_B at 7 T. Simulation according to the Hamiltonian in Equation (1) resulted in the best-fit values of $g_{Co}=2.21$, $D_{Co}=-1.3$ cm^{-1}, and $J=-0.4$ cm^{-1}. Note that the latter value can be underestimated because spin–orbit coupling and crystal-field splitting effects were not included in the model to avoid over-parameterization. Nevertheless, the resulting magnetic behavior is reproduced reasonably well with the proposed model.

For $[Co_2Ni]$, the χT product is 2.08 emu mol^{-1}K at 300 K, which is slightly higher than the sum of spin-only values for two Co^{II} and one Ni^{II} ions. The χT value increases with lowering temperature and reaches a maximum value of 2.71 emu mol^{-1}K at 6 K, indicating ferromagnetic interactions between the Co^{II} and Ni^{II} centers and stabilization of the $S=2$ ground state at low temperatures (Figure 5). The

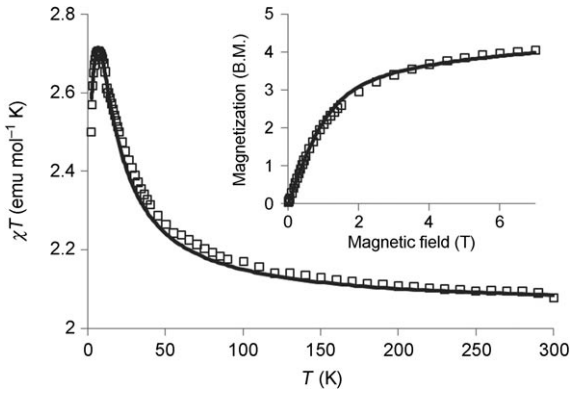

Figure 5. Temperature dependence of the χT product for $[Co_2Ni]$. Inset: Field dependence of magnetization at 1.8 K. The solid lines represent the best fits.

abrupt decrease of χT below 6 K can be attributed to zfs effects and/or intermolecular interactions. The field-dependent magnetization curve attains a maximum value of 4.06 μ_B, which confirms the $S=2$ ground state. The magnetic data were simulated with MAGPACK according to Equation (1), resulting in best-fit values of $g_{Ni}=2.22$, $D=-6$ cm^{-1}, and $J=3.0$ cm^{-1}. An estimate of the ground-state zfs parameter was obtained by fitting the field-dependent magnetization data at different temperatures by using the ANISOFIT program,[46] which yielded $D=-3.4$ cm^{-1} with $g=2.22$. The poor fit of the field- and temperature-dependent magnetization data may be due to the presence of low-lying excited states, which are to be expected given the small magnetic exchange constant. It must be added that an unusually high D value of -8 cm^{-1} was also observed for the previously reported $[Co_2Ni_2]$ square, $\{[Co^{II}(triphos)(CN)_2]_2[Ni^{II}Cl_2]_2\}$[32], which contains the same metal ions as the $[Co_2Ni]$ trimer. Table 6 contains a summary of the magnetic parameters of the $[Co_2M]$ complexes.

Table 6. Summary of magnetic parameters for the trinuclear complexes $[Co_2M]$.

Complex	g_M	D_M [cm^{-1}]	J [cm^{-1}]	Ground state	D_{GS} [cm^{-1}]
$[Co_2Mn]$	2.02	−0.13	−4.8	$S=3/2$	−0.08
$[Co_2Fe]$	2.20	−2.7	−0.6	$S=1$	−1.4
$[Co_2Co]$	2.21	−1.3	−0.4	$S=1/2$	−0.9
$[Co_2Ni]$	2.22	−6	+3.0	$S=2$	−3.4

© 2010 Wiley-VCH Verlag GmbH & Co. KGaA, Weinheim

{[Co(triphos)(CN)$_2$]$_2$[M(MeOH)$_4$]$_2$}(BF$_4$)$_4$ (M=Mn, Ni): The magnetic behavior of [Co_2Mn_2] is virtually identical to that of the tetranuclear cluster, {[Co(triphos)(CN)$_2$]$_2$-[$MnCl_2$]$_2$, previously reported by our group.[32] The χT versus T plot exhibits a room-temperature value of 9.41 emu mol^{-1} K, which is in good agreement with the expected value (9.56 emu mol^{-1} K) for two Co^{II} ($S=1/2$) and two Mn^{II} ions ($S=5/2$) in the absence of magnetic coupling (Figure 6). The value of χT decreases upon cooling until T

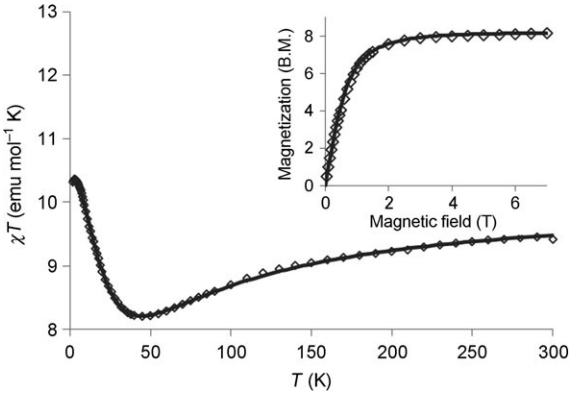

Figure 6. Temperature dependence of the χT product for [Co_2Mn_2]. Inset: Field dependence of magnetization at 1.8 K. The solid lines represent a simulation by using MAGPACK.

$\approx$45 K, indicating antiferromagnetic interactions between the metal sites. Below 45 K, the χT product increases to reach a maximum of 10.36 at 3 K, which is consistent with stabilization of an $S=4$ ground state. The field-dependent magnetization curve measured at 1.8 K reaches the saturation value of 8.16 μ_B, which also supports the presence of an $S=4$ ground state as a result of antiferromagnetic coupling. The data were analyzed by using MAGPACK by treating the interactions between Mn^{II} and Co^{II} spins as isotropic and identical (see Equation (2)).

$$\mathscr{H} = 2\mu_B H_z(g_{Co}S_{z,Co} + g_M S_{z,M}) - 2J(S_{Co1} + S_{Co2}) \cdot (S_{M1} + S_{M2}) + 2D_M[S^2{}_{z,M} - 1/3S_M(S_M + 1)] \quad (2)$$

The resulting best-fit values are $g_{Mn}=2.05$, $D_{Mn}=-0.3$ cm^{-1}, and $J=-6.8$ cm^{-1}. The larger magnetic exchange value as compared with that obtained for the [Co_2Mn] trimer is explained by a smaller degree of distortion of the Co–CN–Mn bridge in [Co_2Mn_2] and hence stronger overlap between the magnetic orbitals of the Co^{II} and Mn^{II} centers.

The χT value of 3.42 emu mol^{-1} K observed for [Co_2Ni_2] at 300 K is slightly higher than the expected value of 2.82 emu mol^{-1} K for two noninteracting low-spin Co^{II} ($S=1/2$) and two Ni^{II} ($S=1$) spin centers, which is attributed to anisotropy of the Ni^{II} ions. Overall, the temperature dependence of χT is similar to that of the Co_2Ni_2 square, {[Co^{II}-(triphos)(CN)$_2$]$_2$[$Ni^{II}Cl_2$]$_2$},[32] in which χT gradually decreases with lowering temperatures owing to antiferromagnetic interactions between the Co^{II} and Ni^{II} ions (Figure 7). The best fit to the theoretical model described by the Hamiltoni-

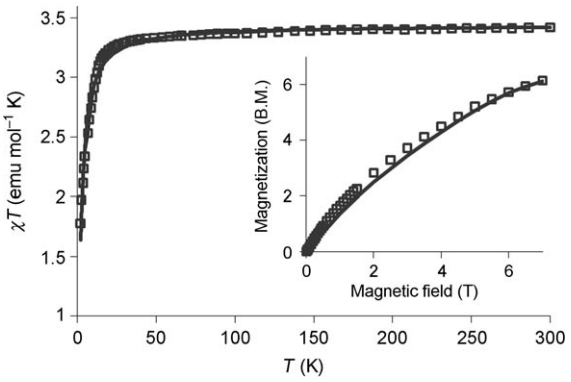

Figure 7. Temperature dependence of the χT product for [Co_2Ni_2]. Inset: Field dependence of magnetization at 1.8 K. The solid lines represent the best fits.

an in Equation (2) was obtained with the parameters $g_{Ni}=2.28$, $D_{Ni}=-1.4$ cm^{-1}, and $J=-0.8$ cm^{-1}. Temperature- and field-dependent magnetization data were simulated with ANISOFIT[44] to yield best-fit parameters of $g=2.28$ and $D_{GS}=-1.4$ cm^{-1} for the $S=1$ ground state (Figure S6 in the Supporting Information).

The most interesting observation in the study of the magnetic properties is that the change in the topology of magnetic centers results in a change in the type of magnetic superexchange from ferromagnetic for the [Co_2Ni] trimer to antiferromagnetic for the [Co_2Ni_2] square. The origin of this surprising difference is expected to be directly related to the overlap of the magnetic orbitals in these clusters, an issue that is not clear from merely examining the structures. To better understand the differences in the magnetic behavior of [Co_2Ni] and [Co_2Ni_2], a computational study by DFT methods was undertaken (a summary of the magnetic properties of the tetranuclear complexes [Co_2M_2] is given in Table 7).

Table 7. Magnetic properties of the tetranuclear complexes [Co_2M_2].

Complex	g_M	D_M [cm^{-1}]	J [cm^{-1}]	Ground state	D_{GS} [cm^{-1}]
[Co_2Mn_2]	2.05	−0.3	−6.8	$S=3/2$	−0.18
[Co_2Ni_2]	2.28	−1.4	−0.8	$S=1$	−0.8

DFT calculations: Singly occupied molecular orbitals, the magnetic orbitals for the highest spin state of the considered systems, can be obtained by DFT calculations. For the sake of simplicity, the phenyl groups of the triphos ligands were replaced with hydrogen atoms. Calculations performed on the mononuclear precursor (Figure S7 in the Supporting Information) and on the family of trinuclear and tetranuclear clusters revealed that the magnetic orbital of the pentacoor-

 © 2010 Wiley-VCH Verlag GmbH & Co. KGaA, Weinheim

dinate Co^{II} ion is located predominantly on the d_{z^2} orbital, which is oriented toward the axial P atom (Figure 8). Figure 9 depicts the magnetic molecular orbitals of the trinuclear clusters located at the M^{II} site. In contrast to previously reported clusters containing e_g type magnetic orbitals that delocalize onto the σ orbital ($3a_1$) of the cyanide ligand, the e_g-like orbital of the Co^{II} ion delocalizes onto the π* orbital (2e) of the cyanide ligand. This conclusion is true for both the trinuclear $[Co_2M]$ and tetranuclear $[Co_2M_2]$ clusters. The orientation of the d_{z^2} orbital, which is not perpendicular to the σ orbital of the cyanide ligand (the P_{axial}-Co-C angle is ≈105°), is responsible for this unusual interaction. On the other hand, the e_g- and t_{2g}-type orbitals located on the central octahedral metal site of the trinuclear clusters interact with the σ and π* orbitals of the cyanide ligand, respectively.

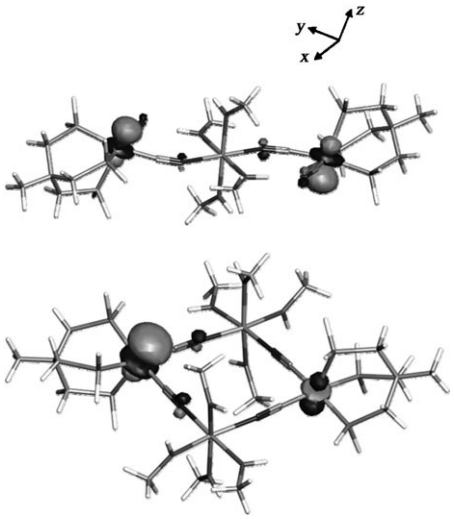

Figure 8. The Co^{II} magnetic molecular orbitals of the trinuclear $[Co_2Ni]$ and tetranuclear $[Co_2Ni_2]$ complexes.

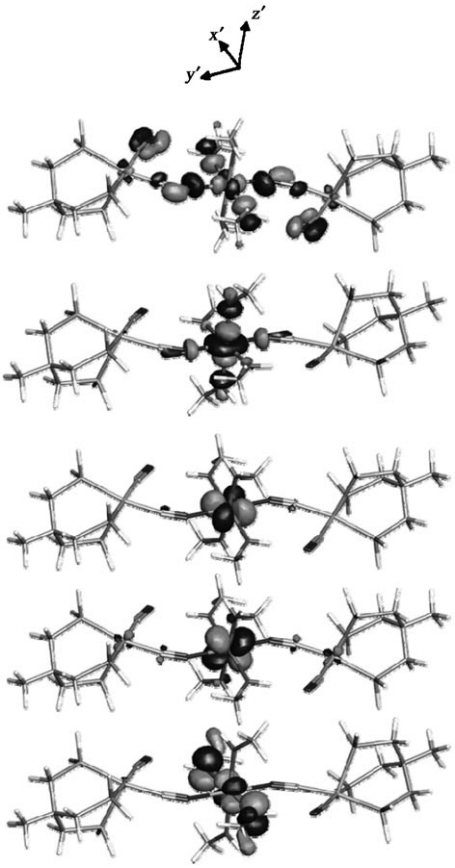

Figure 9. Magnetic molecular orbitals of $[Co_2Mn]$ located on the internal octahedral M^{II} site. For $[Co_2Ni]$, only the two magnetic orbitals at the top are present.

Let us first consider the orbital overlap along the *x* axis of the $[Co_2M]$ trimer, which coincides with the direction of the Co–CN–M bridge. Because the d_{xz} orbital of the central M atom and the d_{z^2} orbital of the Co^{II} site delocalize into the π* orbital of CN^-, antiferromagnetic coupling is predicted between the unpaired spins these orbitals. In addition, a ferromagnetic contribution is also operative because the remaining orbitals of the central M atom delocalize into the other type of cyanide orbital that does not overlap with the magnetic d_{z^2} orbital of the Co^{II} site. Note that the bending of the bridging cyanide ligand increases the overlap of σ and π orbitals the result of which is weaker ferromagnetic coupling between orthogonal orbitals of adjacent metal ions. Therefore, a competition between the antiferromagnetic and ferromagnetic contributions to superexchange is occurring in the trinuclear systems, $[Co_2Mn]$, $[Co_2Fe]$, and $[Co_2Co]$, in which the central atom has unpaired spin density in both e_g- and t_{2g}-type orbitals. The antiferromagnetic contribution dominates, as typically observed in such cases,[16] with the most negative value of the superexchange constant *J* being predicted for the $[Co_2Mn]$ cluster. In contrast, the superexchange interaction between Co^{II} and Ni^{II} ions in $[Co_2Ni]$ should be ferromagnetic owing to the lack of unpaired spins in the t_{2g} type orbitals of the central Ni^{II} ion. These conclusions agree with the experimentally observed behavior of the $[Co_2M]$ complexes (Table 6).

The complex $[Co_2Mn_2]$ behaves similarly to $[Co_2Mn]$ because the same symmetry considerations are also valid for the tetranuclear clusters (Figure 10). The larger exchange coupling value is attributed to the fact that the Co–CN–Mn bridges are less bent for $[Co_2Mn_2]$. In the case of $[Co_2Ni_2]$, the magnetic orbitals delocalize on different orbitals of the cyanide ligand, which implies that ferromagnetic interactions should be dominant, but the magnetic data are in accordance with antiferromagnetic interactions. An examination of the calculated isosurfaces of difference density (Figure 11) allows for an analysis of not only the magnetic orbitals but also spin polarization by comparing the excess α and β spin densities. It was found that excess α spin density is localized on the metal centers and the bridging cyanide ligands. Furthermore, the presence of excess β spin density suggests spin polarization onto the σ orbital of cyanide ligands as well as the $d_{x^2-y^2}$ orbital of Co^{II} sites due to additional spin densities on these orbitals. Such delocalization is not observed for the trinuclear complexes, most likely due

 © 2010 Wiley-VCH Verlag GmbH & Co. KGaA, Weinheim

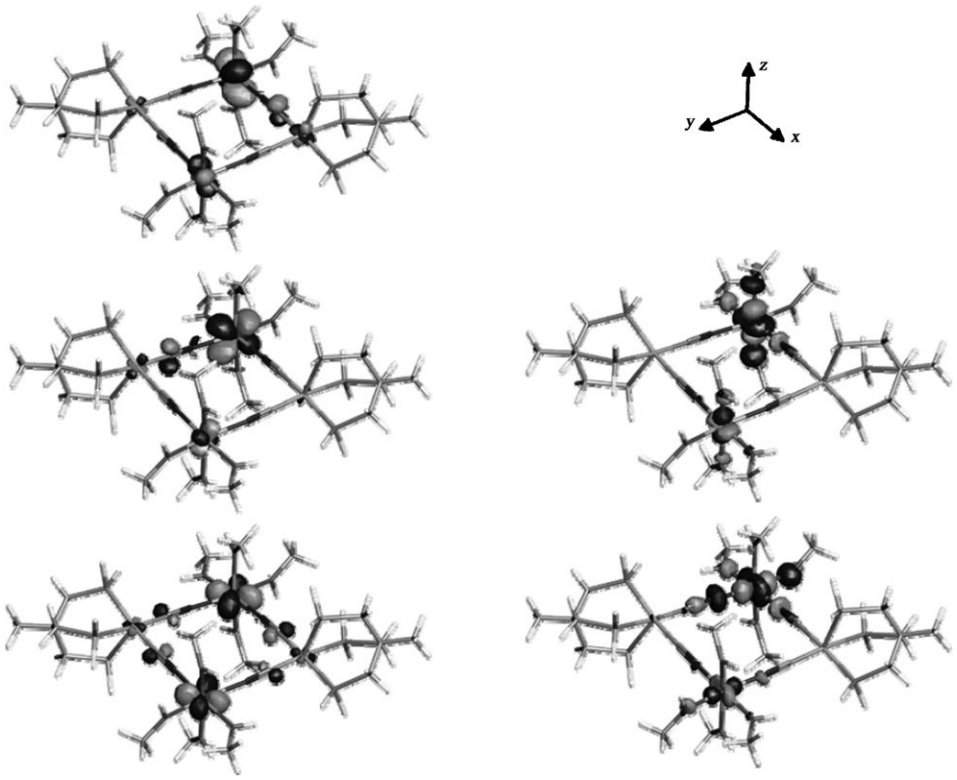

Figure 10. Magnetic molecular orbitals of $[Co_2Mn_2]$ located at the octahedral M^{II} sites.

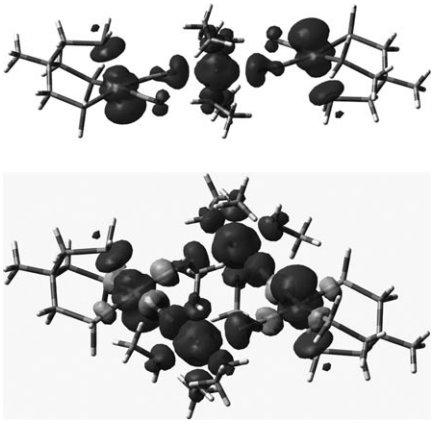

Figure 11. Isosurfaces of difference densities for $[Co_2Ni]$ (top) and $[Co_2Ni_2]$ (bottom). Spin densities of excess α orbitals are represented in dark grey and those of β orbitals are represented in light grey. Spin densities are displayed at an isosurface value of ±0.0015.

to a greater distortion of the Co–CN–M bridge, which serves to restrict the orbital overlap. A possible reason for spin polarization in the tetranuclear $[Co_2Ni_2]$ complex is the interaction of the e_g orbitals of Ni^{II} ion with the $d_{x^2-y^2}$ orbital of Co^{II} sites through the σ orbital of cyanide ligand due to nonorthogonality of these orbitals, which would result in a lowering of the energy of the $d_{x^2-y^2}$ orbital of Co^{II} site and, therefore, mixing of the $d_{x^2-y^2}$ orbital with the e_g orbitals of Co^{II} site. The aforementioned spin polarization is the likely origin of the antiferromagnetic contribution to superexchange in the $[Co_2Ni_2]$ complex. Thus, the weak antiferromagnetic coupling ($J=-0.8\ cm^{-1}$) observed in this complex is a result of competing antiferromagnetic and ferromagnetic interactions between the Ni^{II} and Co^{II} ions mediated by the e_g–$d_{x^2-y^2}$ and e_g–d_{z^2} orbital combinations, respectively.

Conclusion

The use of $[Co^{II}(triphos)(CN)_2]$ as a building block produced a family of cationic trinuclear and tetranuclear complexes. The three trinuclear derivatives $\{[Co^{II}(triphos)(CN)_2]_2[M^{II}(CH_3OH)_4]\}^{2+}$ ($[Co_2M]$) exhibit antiferromagnetic coupling between the Co^{II} and M^{II} centers (M = Mn, Fe, Co) whereas $[Co_2Ni]$ exhibits ferromagnetic coupling. The computational studies provided important insight into the identities and orientations of the magnetic orbitals of the metal centers and their interactions with the orbitals of the cyanide bridging ligands. These results are in good agreement with the magnetic data. Because the antiferromagnetic interaction of the d_{z^2} orbital of the central octahedral metal sites with the magnetic orbital of the Co^{II} ions takes place through the π* orbital of the cyanide ligand, $[Co_2Ni]$ is the only complex that exhibits ferromagnetic superexchange interactions due to a lack of t_{2g}-type magnetic orbitals.

The tetranuclear complex, $\{[Co^{II}(triphos)(CN)_2]_2[Mn(CH_3OH)_4]_2\}^{4+}$ ($[Co_2Mn_2]$) was found to exhibit antiferromagnetic interactions between the metal centers, an observation that is supported by theoretical calculations. In contrast to the cluster $[Co_2Ni]$, which exhibits ferromagnetic behavior, the magnetic properties of $[Co_2Ni_2]$ indicate antiferromagnetic interactions despite the fact that same metal ions interact through the cyanide bridging ligand. The difference in the nature of the magnetic exchange coupling in these Co^{II}–CN–Ni^{II} containing products is explained by examining the isosurfaces of difference density, which suggest that spin polarization is operative for the tetranuclear $[Co_2Ni_2]$ molecule but not for the $[Co_2Ni]$ trinuclear analog due to the acute nature of the M-N-C angle (~145°) in the latter case.

In addition to their interesting magnetic properties, the new complexes are promising building blocks for the systematic preparation of higher nuclearity clusters or extended

 © 2010 Wiley-VCH Verlag GmbH & Co. KGaA, Weinheim

networks. They are soluble in many common polar solvents and possess labile solvent ligands that can be replaced in substitution chemistry unlike most of their trinuclear or tetranuclear counterparts in the literature.

Acknowledgements

This research was supported in part by the National Science Foundation (PI grant CHE-0610019), the Department of Energy (grant DE-FG03-02ER45999) and the Welch Foundation (A-1449). Funding of the CCD diffractometer (CHE-9807975) by the NSF is gratefully acknowledged.

[1] K. R. Dunbar, R. A. Heintz, *Prog. Inorg. Chem.* **1996**, *45*, 283–391.
[2] M. Shatruk, C. Avendano, K. R. Dunbar, *Prog. Inorg. Chem.* **2009**, *56*, 155–334.
[3] D. S. Bieksza, D. N. Hendrickson, *Inorg. Chem.* **1977**, *16*, 924–929.
[4] H. Weihe, H. U. Gudel, *Comments Inorg. Chem.* **2000**, *22*, 75–103.
[5] S. Ferlay, T. Mallah, R. Ouahes, P. Veillet, M. Verdaguer, *Inorg. Chem.* **1999**, *38*, 229–234.
[6] M. Atanasov, C. Busche, P. Comba, F. Hallak, B. Martin, G. Rajaraman, J. Slageren, H. Wadepohl, *Inorg. Chem.* **2008**, *47*, 8112–8125.
[7] V. Marvaud, J. M. Herrera, T. Barilero, F. Tuyeras, R. Garde, A. Scuiller, C. Decroix, M. Cantuel, C. Desplanches, *Monatsh. Chem.* **2003**, *134*, 149–163.
[8] M. Atanasov, P. Comba, C. A. Daul, *J. Phys. Chem. A* **2006**, *110*, 13332–13340.
[9] C. Daul, M. Atanasov, *Chimia* **2005**, *59*, 504–510.
[10] V. Eyert, B. Siberchicot, M. Verdaguer, *Phys. Rev. B* **1997**, *56*, 8959–8969.
[11] O. Kahn, B. Briat, *J. Chem. Soc. Faraday Trans. 2* **1976**, *72*, 268.
[12] O. Kahn, B. Briat, *J. Chem. Soc. Faraday Trans. 2* **1976**, *72*, 1441.
[13] S. Ferlay, T. Mallah, R. Ouahes, P. Veillet, M. Verdaguer, *Nature* **1995**, *378*, 701.
[14] T. Mallah, M. Thiebaut, M. Verdaguer, P. Veillet, *Science* **1993**, *262*, 1554.
[15] J. M. Herrera, A. Bachschmidt, F. Villain, A. Bleuzen, V. Marvaud, W. Wernsdorfer, M. Verdaguer, *Philos. Trans. R. Soc. A* **2008**, *366*, 127–138.
[16] E. Ruiz, A. Rodriguez-Fortea, S. Alvarez, M. Verdaguer, *Chem. Eur. J.* **2005**, *11*, 2135–2144.
[17] V. Marvaud, C. Decroix, A. Scuiller, C. Guyard-Duhayon, J. Vaissermann, F. Gonnet, M. Verdaguer, *Chem. Eur. J.* **2003**, *9*, 1677–1691.
[18] A. Rodríguez-Fortea, P. Alemany, S. Alvarez, E. Ruiz, A. Scuiller, C. Decroix, V. Marvaud, J. Vaissermann, M. Verdaguer, *Inorg. Chem.* **2001**, *40*, 5868–5877.
[19] J. I. Kim, J. H. Yoon, H. Y. Kwak, E. K. Koh, C. S. Hong, *Eur. J. Inorg. Chem.* **2008**, 2756–2763.
[20] M. L. Flay, H. Z. Vahrenkamp, *Eur. J. Inorg. Chem.* **2003**, 1719–1726.
[21] M. Flay, V. Comte, H. Z. Vahrenkamp, *Z. Anorg. Allg. Chem.* **2003**, *629*, 1147–1152.
[22] H. Oshio, H. Onodera, O. Tamada, H. Mizutani, T. Hikichi, T. Ito, *Chem. Eur. J.* **2000**, *6*, 2523–2530.
[23] E. J. Schelter, A. V. Prosvirin, K. R. Dunbar, *J. Am. Chem. Soc.* **2004**, *126*, 15004–15005.
[24] J. L. Heinrich, P. A. Berseth, J. R. Long, *Chem. Commun.* **1998**, 1231–1232.
[25] C.-F. Wang, J.-L. Zuo, B. M. Bartlett, Y. Song, J. R. Long, X.-Z. You, *J. Am. Chem. Soc.* **2006**, *128*, 7162.
[26] L. Toma, R. Lescouezec, J. Vaissermann, F. S. Delgado, C. Ruiz-Perez, R. Carrasco, J. Cano, F. Lloret, M. Julve, *Chem. Eur. J.* **2004**, *10*, 6130–6145.
[27] S. Wang, J.-L. Zuo, H.-C. Zhou, Y. Song, S. Gao, X.-Z. You, *Eur. J. Inorg. Chem.* **2004**, 3681–3687.
[28] J. H. Yoon, J.-H. Lim, H.-C. Kim, C. S. Hong, *Inorg. Chem.* **2006**, *45*, 9613–9615.
[29] R. Rupp, G. Huttner, P. Kircher, R. Soltek, M. Buchner, *Eur. J. Inorg. Chem.* **2000**, 1745–1757.
[30] V. Jacob, S. Mann, G. Huttner, O. Walter, L. Zsolnai, E. Kaifer, P. Rutsch, P. Kircher, E. Bill, *Eur. J. Inorg. Chem.* **2001**, 2625–2640.
[31] F. Karadas, E. J. Schelter, A. V. Prosvirin, J. Bacsa, K. R. Dunbar, *Chem. Commun.* **2005**, 1414–1416.
[32] F. Karadas, E. J. Schelter, M. Shatruk, A. V. Prosvirin, J. Bacsa, D. Smirnow, A. Ozarowski, J. Krzystek, J. Telser, K. R. Dunbar, *Inorg. Chem.* **2008**, *47*, 2074–2082.
[33] Gaussian 03, Revision C.02, M. J. Frisch, G. W. Trucks, H. B. Schlegel, G. E. Scuseria, M. A. Robb, J. R. Cheeseman, J. A. Montgomery, Jr., T. Vreven, K. N. Kudin, J. C. Burant, J. M. Millam, S. S. Iyengar, J. Tomasi, V. Barone, B. Mennucci, M. Cossi, G. Scalmani, N. Rega, G. A. Petersson, H. Nakatsuji, M. Hada, M. Ehara, K. Toyota, R. Fukuda, J. Hasegawa, M. Ishida, T. Nakajima, Y. Honda, O. Kitao, H. Nakai, M. Klene, X. Li, J. E. Knox, H. P. Hratchian, J. B. Cross, V. Bakken, C. Adamo, J. Jaramillo, R. Gomperts, R. E. Stratmann, O. Yazyev, A. J. Austin, R. Cammi, C. Pomelli, J. W. Ochterski, P. Y. Ayala, K. Morokuma, G. A. Voth, P. Salvador, J. J. Dannenberg, V. G. Zakrzewski, S. Dapprich, A. D. Daniels, M. C. Strain, O. Farkas, D. K. Malick, A. D. Rabuck, K. Raghavachari, J. B. Foresman, J. V. Ortiz, Q. Cui, A. G. Baboul, S. Clifford, J. Cioslowski, B. B. Stefanov, G. Liu, A. Liashenko, P. Piskorz, I. Komaromi, R. L. Martin, D. J. Fox, T. Keith, M. A. Al-Laham, C. Y. Peng, A. Nanayakkara, M. Challacombe, P. M. W. Gill, B. Johnson, W. Chen, M. W. Wong, C. Gonzalez, J. A. Pople, Gaussian, Inc., Wallingford CT, **2004**.
[34] A. D. Becke, *Phys. Rev. A* **1988**, *38*, 3098.
[35] A. D. Becke, *J. Chem. Phys.* **1993**, *98*, 5648.
[36] C. Lee, W. Yang, R. G. Parr, *Phys. Rev. B* **1988**, *37*, 785.
[37] W. J. Hehre, L. Radom, P. von R. Schleyer, J. A. Pople, *Ab Initio Molecular Orbital Theory*, Wiley-Interscience, New York, **1986**.
[38] M. Couty, M. B. Hall, *J. Comput. Chem.* **1996**, *17*, 1359–1370.
[39] P. Flukiger, **1992**.
[40] B. J. Hathaway, D. G. Holah, A. E. Underhill, *J. Chem. Soc.* **1962**, 2444–2448.
[41] SMART and SAINT, Siemens Analytical X-ray Instruments Inc., Madison, WI, **1996**.
[42] SADABS, G. M. Sheldrick, University of Göttingen, Göttingen, **1996**.
[43] L. J. Barbour, *J. Supramol. Chem.* **2001**, *1*, 189–191.
[44] Z.-H. Ni, H.-Z. Kou, L.-F. Zhang, W.-W. Ni, Y.-B. Jiang, A.-L. Cui, J. Ribas, O. Sato, *Inorg. Chem.* **2005**, *44*, 9631–9633.
[45] H.-R. Wen, C.-F. Wang, J.-L. Zuo, Y. Song, X.-R. Zeng, X.-Z. You, *Inorg. Chem.* **2006**, *45*, 582–590.
[46] M. P. Shores, J. J. Sokol, J. R. Long, *J. Am. Chem. Soc.* **2002**, *124*, 2279–2292.

Received: January 18, 2010
Published online: May 18, 2010

 © 2010 Wiley-VCH Verlag GmbH & Co. KGaA, Weinheim